

Elastohydrodynamic Synchronization of Rotating Bacterial Flagella

Maria Tătulea-Codrean^{1,2} and Eric Lauga^{1,*}

¹*Department of Applied Mathematics and Theoretical Physics, University of Cambridge, Cambridge CB3 0WA, United Kingdom*

²*Collège de France, 11 place Marcelin Berthelot, 75005 Paris, France*

 (Received 8 July 2021; revised 3 February 2022; accepted 25 March 2022; published 17 May 2022)

To rotate continuously without jamming, the flagellar filaments of bacteria need to be locked in phase. While several models have been proposed for eukaryotic flagella, the synchronization of bacterial flagella is less well understood. Starting from a reduced model of flexible and hydrodynamically coupled bacterial flagella, we rigorously coarse grain the equations of motion using the method of multiple scales, and hence show that bacterial flagella generically synchronize to zero phase difference via an elastohydrodynamic mechanism. Remarkably, the far-field rate of synchronization is maximized at an intermediate value of elastic compliance, with surprising implications for bacteria.

DOI: [10.1103/PhysRevLett.128.208101](https://doi.org/10.1103/PhysRevLett.128.208101)

Motile eukaryotic cells propelled by slender flagella or cilia have long been known to display a feature essential to locomotion: the synchronization of their swimming appendages [1,2]. From nearby spermatozoa matching the beating pattern of their flexible flagella, to ciliary carpets that actively pump fluids in a coordinated fashion, the synchronization of eukaryotic flagella and cilia is ubiquitous [3,4]. Multiple physical factors can induce synchronization, including direct hydrodynamic interactions between the filaments [5,6], elastic coupling through intracellular features [7,8], steric interactions [9], and coupling through the motion of the cell body [10,11]. The mechanisms for synchronization have been uncovered by theoretical studies [12–21], among which a popular minimal approach is to model the tips of eukaryotic flagella and cilia as particles undergoing periodic motion above a rigid surface representing the cell [22–27].

For prokaryotic cells, the question of synchronization is especially important for peritrichous bacteria equipped with multiple propulsion-inducing flagella, such as the model organism *Escherichia coli* [28]: their helical flagellar filaments rotate passively under the actuation of molecular motors embedded in the cell wall and form coherent bundles behind the cell body, pushing the bacterium forward when it swims in a straight “run” [29]. The geometrical constraints imposed by the helical shape require the flagellar filaments to be in phase with each other to form smoothly rotating bundles [30]. The level of synchronization between filaments is expected to influence the propulsive efficiency of the bundle, while intermittent loss of synchronization may contribute to the initiation of “tumble” events [31,32].

Compared to eukaryotic flagella, the fundamental mechanisms of synchronization in rotating bacterial flagella are not yet fully understood. Computational studies have

shown that some form of elastic compliance is necessary in addition to hydrodynamic interactions, since hydrodynamically coupled helices rotating rigidly about a fixed axis do not synchronize [33,34]. Simulations have also revealed that the balance between bundling and synchronization times depends strongly on the initial separation between the filaments [35] and that filaments may slip out of synchrony if driven by unequal torques [32]. Experimental studies on the synchronization of rotating bodies include systems of light-driven microrotors [36] and of macroscopic-scale rotating paddles [37].

In this Letter, we provide a microscopic physical model for the dynamics of compliant bacterial flagella and use the method of multiple scales to rigorously coarse grain the equations of motion for two flagella interacting in the far field into an evolution equation for their mean phase difference. The model, illustrated in Fig. 1, preserves the salient features of the bacterial flagellum: the rotary motor operating near constant torque [38], the left-handed helical shape of the semi-rigid flagellar filament [39], and the flexible connection between motor and filament via the flagellar hook [40]. In contrast to empirical models, our bottom-up approach includes all geometrical and dynamical details, thereby allowing us to derive the explicit dependence of the synchronization rate on the shape and dynamical properties of the bacterial flagellum. The theoretical predictions of our model are verified by numerical simulations (Fig. 2), are shown to remain relevant beyond the far-field limit [41], and are elucidated by a physically intuitive explanation of the mechanism for synchronization, which emerges from the elastohydrodynamic balance on individual filaments (Fig. 3). Remarkably, we show that the rate of synchronization is maximized at intermediate values of elastic compliance, with significant implications for the biophysics of swimming bacteria.

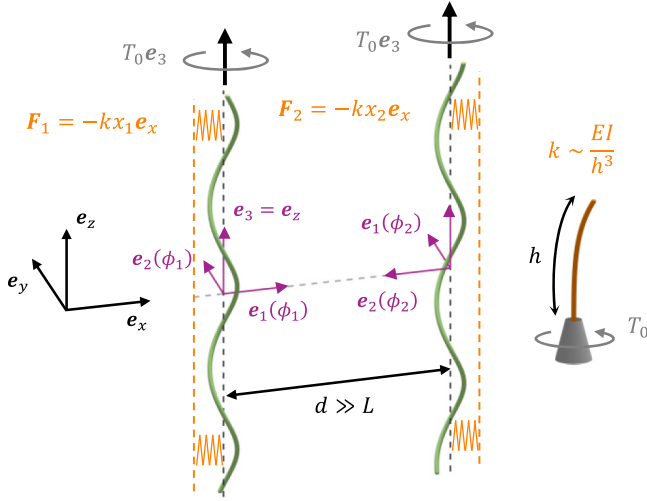


FIG. 1. Reduced model of interacting bacterial flagella. Two parallel helical filaments have phase angles ϕ_j . A constant torque, $T_0 \mathbf{e}_z$, rotates each filament about its axis, while an elastic restoring force, $-kx_j \mathbf{e}_x$, pulls the axis back to a reference position. The tethering points are separated along x by a distance much greater than the length of the filaments, $d \gg L$.

To model the far-field interactions between bacterial flagella, we consider two identical and parallel rigid helices of length L , each rotating in a viscous fluid (viscosity μ) under a constant torque T_0 . The reference positions of the axes are separated by a distance $|\mathbf{d}| = d \gg L$ along the x direction (see Fig. 1). We rescale lengths, forces, and time such that $L = 2$, $\mu = 1$, and $T_0 = 1$ in dimensionless terms. On the microscopic scale of bacteria, the Reynolds numbers are very small so we operate within the framework of Stokes flow, where the relationship between the dynamics (forces \mathbf{F}_j and torques \mathbf{T}_j) and kinematics (linear and angular velocities \mathbf{U}_j and $\mathbf{\Omega}_j$) of rigid bodies is linear. For two flagellar filaments with phase angles ϕ_1 and ϕ_2 , this means

$$\begin{pmatrix} \mathbf{F}_1 \\ \mathbf{T}_1 \end{pmatrix} = \mathbf{S}(\mathbf{d}, \phi_1, \phi_2) \begin{pmatrix} \mathbf{U}_1 \\ \mathbf{\Omega}_1 \end{pmatrix} + \mathbf{C}(\mathbf{d}, \phi_1, \phi_2) \begin{pmatrix} \mathbf{U}_2 \\ \mathbf{\Omega}_2 \end{pmatrix}, \quad (1)$$

where the resistance matrices \mathbf{S} and \mathbf{C} provide the self-induced dynamics and the cross interactions between filaments. In previous work [42], we demonstrate that $\mathbf{S}(\mathbf{d}, \phi_1, \phi_2) = \mathbf{S}_0(\phi_1) + \mathcal{O}(d^{-2})$ when $d \gg L = 2$, where $\mathbf{S}_0(\phi)$ is the resistance matrix for a filament in an infinite fluid, and is obtained by rotating $\mathbf{S}_0(0) = (\mathbf{A}, \mathbf{B}; \mathbf{B}^T, \mathbf{D})$ through an angle ϕ about the vertical axis. Meanwhile $\mathbf{C}(\mathbf{d}, \phi_1, \phi_2) = d^{-1} \mathbf{C}_1(\mathbf{e}_x, \phi_1, \phi_2) + \mathcal{O}(d^{-2})$ and the first-order correction comes from the leading-order expansion of the Oseen tensor, $\mathbf{C}_1(\mathbf{e}_x, \phi_1, \phi_2) = -\mathbf{S}_0(\phi_1)(\mathbf{I} + \mathbf{e}_x \mathbf{e}_x) \cdot \mathbf{S}_0(\phi_2)/(8\pi\mu)$.

To model the elastic link between the flagellar filament and the rotary motor via the flexible hook, as well as the elastic compliance of the semi-rigid filaments, we allow the

axis of each filament to move along x while a linear elastic force (dimensionless strength k) restores it to a reference position (see Fig. 1). The kinematics of helix j is therefore described by two degrees of freedom: lateral displacement, x_j , and phase, ϕ_j . Projecting Eq. (1) onto the four degrees of freedom in our model, we obtain the reduced system up to $\mathcal{O}(d^{-1})$,

$$\begin{pmatrix} -kx_1 \\ T_0 \end{pmatrix} = \tilde{\mathbf{S}}_0(\phi_1) \begin{pmatrix} \dot{x}_1 \\ \dot{\phi}_1 \end{pmatrix} + d^{-1} \tilde{\mathbf{C}}_1(\mathbf{e}_x, \phi_1, \phi_2) \begin{pmatrix} \dot{x}_2 \\ \dot{\phi}_2 \end{pmatrix}, \quad (2)$$

where tildes denote the appropriate subset of rows and columns from the matrices \mathbf{S}_0 and \mathbf{C}_1 .

We next exploit the separation of timescales that occurs at large interfilament distance between fast rotation and slow synchronization. We introduce a slow variable $\tau = d^{-1}t$ alongside the fast variable t for rotation. The solution is then formally expanded as $\phi_j(t) = \phi_j^{(0)}(t, \tau) + d^{-1} \phi_j^{(1)}(t, \tau) + \mathcal{O}(d^{-2})$ with time derivative $\dot{\phi}_j(t) = \phi_{j,t}^{(0)} + d^{-1}(\phi_{j,\tau}^{(0)} + \phi_{j,t}^{(1)}) + \mathcal{O}(d^{-2})$, where subscripts t and τ denote partial derivatives; a similar multiple scale expansion applies to lateral displacements, x_j . Following the method of multiple scales [43], we solve Eq. (2) at zero and first order in d^{-1} . At each order in d^{-1} we further expand the solution in powers of a nested parameter $(\pi N)^{-1} \ll 1$, with N being the number of helical turns (for a typical bacterial flagellar filament $(\pi N)^{-1} \approx 0.1$). This allows us to integrate the equations at each order analytically (full calculations available in Supplemental Material [41]).

At leading order in d^{-1} , the solution of Eq. (2) is that each filament rotates with fixed angular velocity $\mathbf{\Omega}_0 = T_0 D_{33}^{-1}$ as $\phi_j^{(0)}(t, \tau) = \hat{\phi}_j(\tau) + \mathbf{\Omega}_0 t$, where $\hat{\phi}_j(\tau)$ is a constant of integration. Meanwhile, each filament axis oscillates as $x_j^{(0)}(t, \tau) \approx \rho(K) \cos[\phi_j^{(0)} - \xi(K)]$ with amplitude $\rho(K) = B_{23} A_0^{-1} (K^2 + 1)^{-1/2}$ and phase lag $\xi(K) = \tan^{-1}(-K) \in (\pi/2, \pi)$ behind $\phi_j^{(0)}$, where A_{ij}, B_{ij}, D_{ij} are the components of $\mathbf{S}_0(0)$ and $A_0 = (A_{11} + A_{22})/2$. The dimensionless parameter $K = (T_0^{-1} D_{33}) / (k^{-1} A_0) \equiv t_{\text{rot}} / t_{\text{elast}}$ encapsulates the dynamics of actuation (elastic compliance and driving torque) and represents the ratio between the rotation timescale and the elastic relaxation timescale of the flagellum.

At first order in d^{-1} , Eq. (2) can be reduced to a system for $\phi_1^{(0)}$ and $x_1^{(1)}$ only, by substituting the leading-order solution for $x_j^{(0)}$ and applying the solvability condition that the first-order correction $\phi_1^{(1)}$ remains bounded for large t . After some algebra, we deduce the slow evolution of the phase difference, $\Delta\phi = \phi_2^{(0)} - \phi_1^{(0)}$, to be $\Delta\phi_\tau = -k B_{23} (A_0 D_{33})^{-1} (x_1^{(1)} \sin \phi_1^{(0)} - x_2^{(1)} \sin \phi_2^{(0)})$, where the

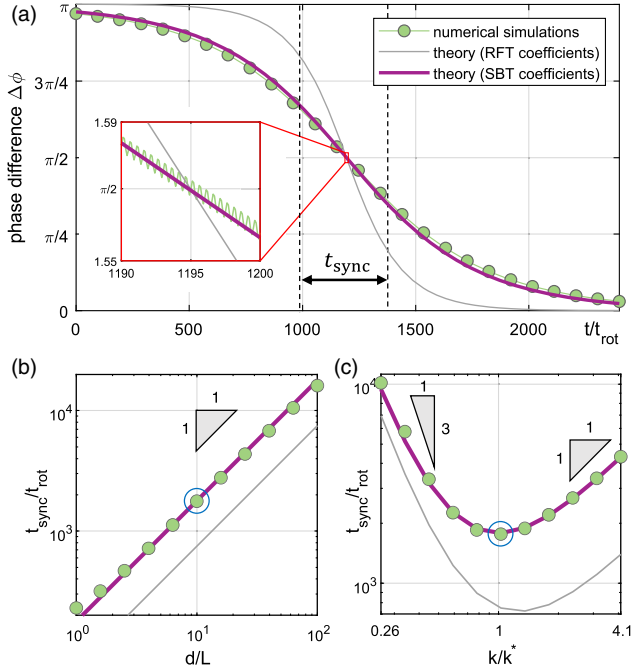


FIG. 2. Interacting bacterial flagella generically synchronize in-phase via an elasto-hydrodynamic mechanism. (a) Evolution of phase difference on the slow time scale of synchronization and (inset) on the fast time scale of rotation, for inter-filament distance $d = 2L$. The timescale for synchronization is (b) proportional to the hydrodynamic coupling between the filaments and (c) minimized at intermediate elastic compliance. Data points circled in blue represent identical input parameters (pitch angle $\psi = 0.446$ and filament thickness $\epsilon = 0.0038$ correspond to a “normal” flagellar filament [29]; full list of parameters available in the Supplemental Material [41]).

first-order perturbation to sideways displacements has the general solution $x_1^{(1)}(t, \tau) = \gamma \sin(\phi_1^{(0)}) + \delta \cos(\phi_1^{(0)}) + \zeta \sin(\phi_2^{(0)}) + \eta \cos(\phi_2^{(0)})$ once the initial transients have decayed exponentially.

By averaging the evolution equation for $\Delta\phi$ over the fast timescale, we exactly recover the classical Adler equation [44] for the mean phase difference $\langle \Delta\phi \rangle_\tau = -kB_{23}(A_0D_{33})^{-1}\eta \sin(\Delta\phi) \equiv -\tau_{\text{sync}}^{-1} \sin(\Delta\phi)$. This leads generically to in-phase synchronization as $\langle \Delta\phi \rangle = 2\tan^{-1}[\tan(\Delta\phi_0/2)\exp(-\tau/\tau_{\text{sync}})]$ [Fig. 2(a)]. Importantly, by identifying the coefficient η in the solution for $x_1^{(1)}$, we can predict the timescale for synchronization $t_{\text{sync}} = d\tau_{\text{sync}} = 2\pi\mu dD_{33}^2(B_{23}^2T_0)^{-1}(K^2 + 1)^2K^{-3}$, which depends explicitly on the actuation dynamics through K and on the helical shape through the individual viscous resistance coefficients A_0 , B_{23} , and D_{33} . Notably, $t_{\text{sync}} \propto (K^2 + 1)^2K^{-3}$ is minimized at an optimum value, $K^* = \sqrt{3}$, independent of distance.

To validate our multiple-scale approach, we compute the instantaneous hydrodynamic forces on the two filaments

using Johnson’s slender-body theory (SBT) [45] and then time step using Runge-Kutta RK4. We include the full hydrodynamic interactions between the filaments by solving the integral equation $8\pi\mu\mathbf{u}_1(s) = \mathcal{L}[\mathbf{f}_1(s)] + \mathcal{K}[\mathbf{f}_1(s')] + \mathcal{J}[\mathbf{f}_2(s'), \mathbf{d}]$, where \mathbf{u}_j and \mathbf{f}_j are the velocity and force density along filament j , \mathcal{L} , and \mathcal{K} represent local and nonlocal effects on the same filament, and the integral operator \mathcal{J} contains the Stokeslet and source dipole flows generated by the other filament [46]. The integral equation is solved numerically using a Galerkin method with Legendre polynomials [42]. Further details of the computational method are available in the Supplemental Material [41]. The final expression for t_{sync} , with A_0 , B_{23} , and D_{33} evaluated either analytically via resistive-force theory (RFT) [47–49] or computationally via SBT [45], is compared against full numerical simulations in Fig. 2. Our multiple-scale theory with SBT coefficients is in perfect agreement with simulations, while RFT captures all qualitative features of synchronization.

Our model of interacting bacterial flagella was coarse-grained using multiple scales and shown to reduce to the Adler equation, leading to in-phase locking. What is the physical mechanism responsible for this flagellar synchronization, and why is synchronization fastest at intermediate values of elastic compliance?

To convey physical intuition, we focus on the details of hydrodynamic forces and allow the filaments to move in a 2D elastic trap (the 1D/2D trap were confirmed to be qualitatively identical via numerical simulations). Since both rotation and lateral displacement occur in the plane perpendicular to the filament axis, it suffices to consider the flows and forces acting on the horizontal projection of the helical centreline. When projected, each helical flagellar filament maps onto a circle. If the helix has a noninteger number of turns, we have a surplus of filament on one side of the circle, so the filament generically reduces to the arc of a circle, or a “horseshoe” (Fig. 3).

We first describe, in Figs. 3(a)–3(d), the intrinsic dynamics of an elastically tethered and rotating horseshoe in the absence of hydrodynamic interactions. A rotating horseshoe with phase angle ϕ defined as in Fig. 3(a) experiences a net viscous drag in the negative $\mathbf{e}_\phi(\phi)$ direction due to a one-sided surplus in force [Fig. 3(a)]. For weak elastic stiffness [$k \ll 1$, Fig. 3(b)], this viscous drag due to rotation is balanced out primarily by the viscous drag due to translation, and thus we have $\dot{\mathbf{x}} \propto -\mathbf{e}_\phi(\phi)$. In contrast, for strong elastic stiffness [$k \gg 1$, Fig. 3(c)], the viscous drag from rotation is balanced primarily by the elastic restoring force, and therefore we have $\mathbf{x} \propto -\mathbf{e}_\phi(\phi)$. In the intermediate regime [$k = O(1)$, Fig. 3(d)], the center of the projected filament oscillates on circular orbits lagging behind the phase ϕ by an angle between $\pi/2$ and π . Importantly, the force exerted by the filament on the fluid, $\mathbf{F} = -k\mathbf{x} = \alpha\mathbf{e}_r(\phi) + \beta\mathbf{e}_\phi(\phi)$, always has a positive \mathbf{e}_r component.

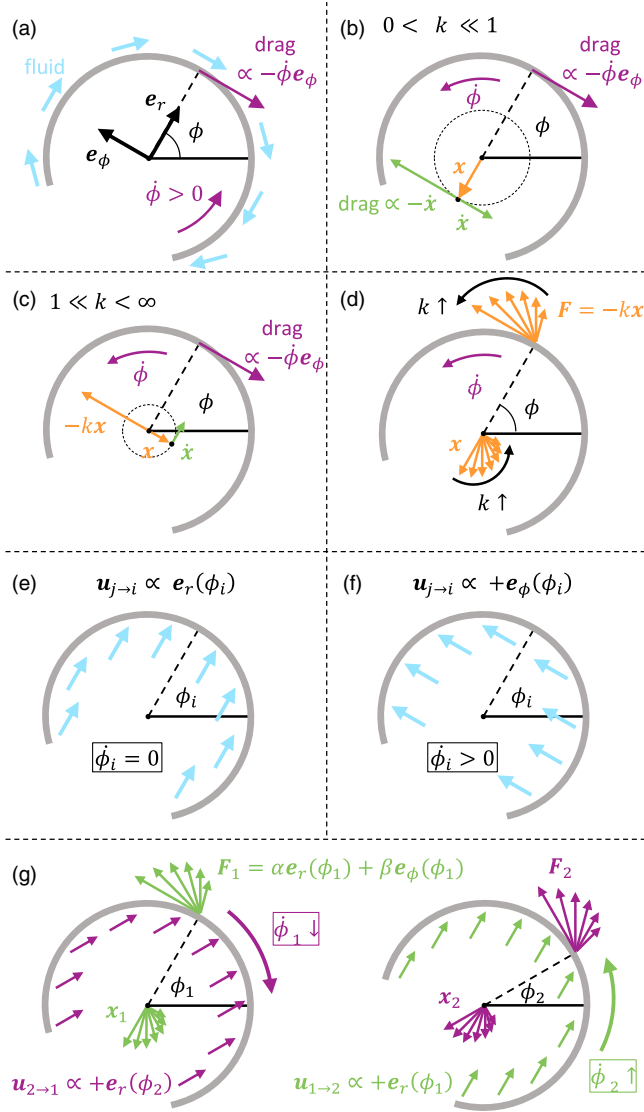


FIG. 3. Physical mechanism for elasto-hydrodynamic synchronization. (a) The viscous drag on a rotating helix with phase angle ϕ is balanced out primarily by (b) the viscous drag due to translation ($k \ll 1$) or (c) by the elastic restoring force ($k \gg 1$). (d) For general values of k , the axis of the helix, \mathbf{x} , lags behind the phase angle ϕ by an angle between $\pi/2$ and π . (e),(f) Filament i speeds up only if the flow induced by filament $j \neq i$ has a positive $\mathbf{e}_\phi(\phi_i)$ component. (g) Hydrodynamically coupled helices synchronize in phase due to the flows that each filament j produces along the positive $\mathbf{e}_r(\phi_j)$ direction and the resulting hydrodynamic stresses on filament $i \neq j$.

To reveal the evolution of the phase difference for interacting helices, we consider in Figs. 3(e)–3(g) how horseshoe i responds to the flows induced by horseshoe $j \neq i$. If the external flow created by filament j near filament i is parallel to $\mathbf{e}_r(\phi_i)$, then the hydrodynamic forces are balanced by symmetry and the external flow does not lead to additional rotation [Fig. 3(e)]. If, however, the flow induced by filament j has a positive $\mathbf{e}_\phi(\phi_i)$

component, then filament i experiences a hydrodynamic torque and speeds up [Fig. 3(f)]. In the far field, the flow induced by filament j at the position of filament i is a uniform flow $\mathbf{F}_j \cdot (\mathbf{I} + \mathbf{e}_x \mathbf{e}_x) / 8\pi\mu d$ (the leading order expansion of a Stokeslet flow). The $\mathbf{e}_\phi(\phi_j)$ component of \mathbf{F}_j leads to a symmetric term $\beta \mathbf{e}_\phi(\phi_i) \cdot (\mathbf{I} + \mathbf{e}_x \mathbf{e}_x) \cdot \mathbf{e}_\phi(\phi_j)$ on both filaments that does not modify the phase difference. In contrast, the flow induced by the positive $\mathbf{e}_r(\phi_j)$ component of \mathbf{F}_j does lead to synchronization: as sketched in Fig. 3(g), these flow components have the effect of slowing down the filament that is ahead and speeding up the one that is behind. This elasto-hydrodynamic balance is the physical mechanism responsible for the synchronization of bacterial filaments.

The phase dynamics illustrated theoretically and numerically in Figs. 2(b)–2(c) are fully explained by the physical mechanism outlined above: (i) the rate of synchronization decays linearly with d , a signature of Stokeslet flows, and (ii) the rate of synchronization is proportional to the radial component of the force, $\alpha = \mathbf{F}_j \cdot \mathbf{e}_r(\phi_j)$, which is largest for intermediate values of k since $\alpha \ll 1$ when either $k \ll 1$ or $k \gg 1$, because $\mathbf{F}_j \approx 0$ or $\mathbf{F}_j \propto \mathbf{e}_\phi(\phi_j)$, respectively, [Fig. 3(d)].

Previous biophysical models of ciliary synchronization assumed $K = t_{\text{rot}}/t_{\text{elast}}$ to be very large [23,27,37]. While this is suitable for eukaryotic flagella, the dynamical properties of bacterial flagella are qualitatively different. Crucially, the bacterial flagellum has two components with bending stiffness separated by four orders of magnitude: $EI_{\text{hook}} \approx 1.6 \times 10^{-4} \text{ pN}\mu\text{m}^2$ [40] and $EI_{\text{filament}} \approx 3.5 \text{ pN}\mu\text{m}^2$ [50]. On dimensional grounds, we have $k \sim EI/h^3$, where EI and h are the bending stiffness and length of the deforming component (hook or filament). We estimate that $K_{\text{hook}} \approx 0.05$, which is significantly below the optimum $K^* = \sqrt{3}$ and gives $t_{\text{sync}}/t_{\text{opt}} = \mathcal{O}(10^3)$ due to the rapid increase of $t_{\text{sync}} \sim K^{-3}$ for small K . However, the finite size of the hook ($h = 59 \text{ nm}$ [40]) likely requires that the proximal end of the flagellar filament deforms as well. For a length scale of deformation around $h = 0.1\text{--}1 \mu\text{m}$, we estimate that $K_{\text{filament}} = 0.2\text{--}200$, a range which straddles the optimum. Surprisingly, this suggests that the comparatively smaller elastic compliance of the semirigid flagellar filament [50], together with the short length [51] and the dynamic stiffening of the flagellar hook [52] could play a crucial role in the synchronization and stability of bacterial flagellar bundles.

The physical mechanism revealed by our reduced model of the bacterial flagellum is distinct from previously proposed eukaryotic mechanisms based on orbital compliance [23] and phase-dependent forcing [26]. It is similar to the axial-compliance mechanism in Ref. [37], but the resulting dynamics of synchronization are qualitatively different due to the specific hydrodynamic resistance of the helical filament. Since the helical amplitude of a

bacterial flagellar filament is much smaller than its length, its resistance to rotation, D_{33} , is much smaller than its resistance to translation, A_0 . This leads to intrinsic kinematics of an individual filament [Figs. 3(b)–3(d)] that cannot be captured by spherical-bead models.

One limitation of our analytical theory is that each filament moves with only two degrees of freedom. Computations for filaments with all six degrees of freedom [41] reveal that the physical mechanism for synchronization is robust against deviations in the axes of the filaments, and that our result for t_{sync} can be modified to take into account a finite angle of inclination between the two filaments (as observed during flagellar bundling). Crucially, the optimum elastic compliance for synchronization is not affected by the inclination.

Another constraint that can be relaxed, even analytically, is the assumption that the filaments are identical [41]. The Adler equation can be modified to include a small mismatch, $\Delta\Omega_0$, in the intrinsic rotation rates of the two filaments, giving $\langle\Delta\phi\rangle_\tau = \Delta\Omega_0 - \tau_{\text{sync}}^{-1} \sin(\Delta\phi)$. The filaments then phase lock to $\Delta\phi_\infty = \sin^{-1}(\Delta\Omega_0\tau_{\text{sync}})$, up to a critical point where the mismatch cannot be compensated by hydrodynamic interactions. This prediction agrees with numerical simulations for two filaments with either mismatched driving torques or different filament geometries.

To make analytical progress, it is often necessary to assume that hydrodynamically coupled bodies are far apart [5,23,25,37]. Despite such constraints, far-field theories are crucial for understanding the underlying principles of synchronization. Here, the theory allowed us to provide a detailed physical mechanism based on an elasto-hydrodynamic balance at the level of individual filaments, which remains valid beyond the far-field limit [41]. The current theory and simulations highlight the essential role played by the elasticity of both the hook and the flagellar filament in the synchronization of bacterial flagella. Numerical simulations beyond the far-field limit [41] suggest that the far-field optimum value of K could distinguish between different near-field trends for t_{sync} . In turn, this could guide future studies into the synchronization of bacterial flagella separated by distances smaller than the filament length, e.g., during flagellar bundling. Our results will enable a comparative analysis of synchronization for the different polymorphic shapes of bacterial flagellar filaments [39], while our methodology can also be used to investigate the impact of the torque-speed relationship of the rotary motor on synchronization [38]. Finally, the noisy Adler equation has been proposed to model the fluctuating dynamics of beating filaments [18,53], so adding noise to the system studied here could enable a better understanding of flagellar unbundling [29].

We gratefully acknowledge funding from the University of Cambridge (George and Lillian Schiff Studentship

supporting M. T. C.), from Collège de France (A. T. E. R. contract supporting M. T. C.), and from the European Research Council through the European Union's Horizon 2020 research and innovation programme (under Grant Agreement No. 682754 to E. L.).

*e.lauga@damtp.cam.ac.uk

- [1] J. Gray, *Ciliary Movement* (Cambridge University Press, Cambridge, England, 1928).
- [2] H. Machemer, *J. Exp. Biol.* **57**, 239 (1972).
- [3] D. Bray, *Cell Movements* (Garland Publishing, New York, 2000).
- [4] E. Lauga, *The Fluid Dynamics of Cell Motility* (Cambridge University Press, Cambridge, England, 2020).
- [5] D. R. Brumley, K. Y. Wan, M. Polin, and R. E. Goldstein, *eLife* **3**, e02750 (2014).
- [6] J. Elgeti and G. Gompper, *Proc. Natl. Acad. Sci. U.S.A.* **110**, 4470 (2013).
- [7] G. Quaranta, M.-E. Aubin-Tam, and D. Tam, *Phys. Rev. Lett.* **115**, 238101 (2015).
- [8] K. Y. Wan and R. E. Goldstein, *Proc. Natl. Acad. Sci. U.S.A.* **113**, E2784 (2016).
- [9] R. Chelakkot, M. F. Hagan, and A. Gopinath, *Soft Matter* **17**, 1091 (2021).
- [10] V. F. Geyer, F. Jülicher, J. Howard, and B. M. Friedrich, *Proc. Natl. Acad. Sci. U.S.A.* **110**, 18058 (2013).
- [11] R. R. Bennett and R. Golestanian, *New J. Phys.* **15**, 075028 (2013).
- [12] S. Gueron, K. Levit-Gurevich, N. Liron, and J. J. Blum, *Proc. Natl. Acad. Sci. U.S.A.* **94**, 6001 (1997).
- [13] G. J. Elfring and E. Lauga, *Phys. Fluids* **23**, 011902 (2011).
- [14] G. J. Elfring and E. Lauga, *J. Fluid Mech.* **674**, 163 (2011).
- [15] S. D. Olson and L. J. Fauci, *Phys. Fluids* **27**, 121901 (2015).
- [16] R. E. Goldstein, E. Lauga, A. I. Pesci, and M. R. E. Proctor, *Phys. Rev. Fluids* **1**, 073201 (2016).
- [17] H. Guo, L. Fauci, M. Shelley, and E. Kanso, *J. Fluid Mech.* **836**, 304 (2018).
- [18] B. Chakrabarti and D. Saintillan, *Phys. Rev. Lett.* **123**, 208101 (2019).
- [19] Y. Man and E. Kanso, *Phys. Rev. Lett.* **125**, 148101 (2020).
- [20] H. Guo, Y. Man, K. Y. Wan, and E. Kanso, *J. R. Soc. Interface* **18**, 20200660 (2021).
- [21] W. Liao and E. Lauga, *Phys. Rev. E* **103**, 042419 (2021).
- [22] A. Vilfan and F. Jülicher, *Phys. Rev. Lett.* **96**, 058102 (2006).
- [23] T. Niedermayer, B. Eckhardt, and P. Lenz, *Chaos* **18**, 037128 (2008).
- [24] D. R. Brumley, M. Polin, T. J. Pedley, and R. E. Goldstein, *Phys. Rev. Lett.* **109**, 268102 (2012).
- [25] N. Uchida and R. Golestanian, *Phys. Rev. Lett.* **106**, 058104 (2011).
- [26] N. Uchida and R. Golestanian, *Eur. Phys. J. E* **35**, 135 (2012).
- [27] I. Tanasijevic and E. Lauga, *Phys. Rev. E* **103**, 022403 (2021).
- [28] H. C. Berg, *E. coli in Motion* (Springer-Verlag, New York, 2004).

- [29] L. Turner, W. S. Ryu, and H. C. Berg, *J. Bacteriol.* **182**, 2793 (2000).
- [30] R. M. Macnab, *Proc. Natl. Acad. Sci. U.S.A.* **74**, 221 (1977).
- [31] N. C. Darnton, L. Turner, S. Rojevsky, and H. C. Berg, *J. Bacteriol.* **189**, 1756 (2007).
- [32] S. Y. Reigh, R. G. Winkler, and G. Gompper, *PLoS One* **8**, e70868 (2013).
- [33] M. J. Kim and T. R. Powers, *Phys. Rev. E* **69**, 061910 (2004).
- [34] M. Reichert and H. Stark, *Eur. Phys. J. E* **17**, 493 (2005).
- [35] S. Y. Reigh, R. G. Winkler, and G. Gompper, *Soft Matter* **8**, 4363 (2012).
- [36] R. Di Leonardo, A. Búzás, L. Kelemen, G. Vizsnyiczai, L. Oroszi, and P. Ormos, *Phys. Rev. Lett.* **109**, 034104 (2012).
- [37] B. Qian, H. Jiang, D. A. Gagnon, K. S. Breuer, and T. R. Powers, *Phys. Rev. E* **80**, 061919 (2009).
- [38] Y. Sowa and R. M. Berry, *Q. Rev. Biophys.* **41**, 103 (2008).
- [39] K. Hasegawa, I. Yamashita, and K. Namba, *Biophys. J.* **74**, 569 (1998).
- [40] A. Sen, R. K. Nandy, and A. N. Ghosh, *J. Electron Microsc.* **53**, 305 (2004).
- [41] See Supplemental Material at <http://link.aps.org/supplemental/10.1103/PhysRevLett.128.208101> for details of the analytical calculations, details of the computational method, additional numerical results, and a list of the simulation parameters.
- [42] M. Tătulea-Codrean and E. Lauga, *Phys. Rev. Fluids* **6**, 074103 (2021).
- [43] E. J. Hinch, *Perturbation Methods* (Cambridge University Press, Cambridge, England, 1991).
- [44] R. Adler, *Proc. IRE* **34**, 351 (1946).
- [45] R. E. Johnson, *J. Fluid Mech.* **99**, 411 (1980).
- [46] A. K. Tornberg and M. J. Shelley, *J. Comput. Phys.* **196**, 8 (2004).
- [47] G. Hancock, *Proc. R. Soc. A* **217**, 96 (1953).
- [48] J. Gray and G. J. Hancock, *J. Exp. Biol.* **32**, 802 (1955).
- [49] J. Lighthill, *SIAM Rev.* **18**, 161 (1976).
- [50] N. C. Darnton and H. C. Berg, *Biophys. J.* **92**, 2230 (2007).
- [51] I. Spöring, V. A. Martinez, C. Hotz, J. Schwarz-Linek, K. L. Grady, J. M. Nava-Sedeño, T. Vissers, H. M. Singer, M. Rohde, C. Bourquin, H. Hatzikirou, W. C. K. Poon, Y. S. Dufour, and M. Erhardt, *PLoS Biol.* **16**, e2006989 (2018).
- [52] A. L. Nord, A. Biquet-Bisquert, M. Abkarian, T. Pigaglio, F. Seduk, A. Magalon, and F. Pedaci, *arXiv:2106.15435*.
- [53] R. E. Goldstein, M. Polin, and I. Tuval, *Phys. Rev. Lett.* **103**, 168103 (2009).